Available online at https://link.springer.com/journal/42241
http://www.jhydrodynamics.com
Journal of Hydrodynamics, 2022, 34(1): 148-155
https://doi.org/10.1007/s42241-022-0015-6

Analysis of the spanwise vortex of open channel flows based on the Omega-Liutex vortex identification method

Bin Li[1, 2], Wen-jun Yang[1*], Jie Li[1], Si-yu Jing[1], Yue Chen[3]
1. *Changjiang River Scientific Research Institute, Wuhan 430010, China*
2. *Fujian College of Water Conservancy and Electric Power, Sanming 353000, China*
3. *Department of Water Conservancy and Hydropower Engineering, Hohai University, Nanjing 210098, China*

(Received December 21, 2020, Revised January 13, 2021, Accepted January 22, 2021, Published online February 25, 2022)

Abstract: In this paper, a particle imaging velocimetry (PIV) system of high-temporal-spatial resolution is used to investigate the spanwise vortex distribution of fully developed turbulent flows in an open channel and its relationship with the turbulence. The distributions of the time-averaged velocity, the turbulence intensity and the Reynolds stress are obtained in the longitudinal profile. The third-generation vortex identification method (based on the Omega-Liutex vector) is applied to accurately identify and analyze the vortex in the spanwise direction. The results suggest that the vortex density increases with the Reynolds number at a given aspect ratio (B/H) of the flow. The distribution trend of the spanwise vortex density in the vertical direction remains unchanged for different discharges. Specifically, the vortex density increases along the vertical direction and reaches the peak at $y/H = 0.15$, then decreases and reaches the bottoms at the flow surface.

Key words: Open channel turbulent flows, spanwise vortex, Reynolds number, particle imaging velocimetry (PIV), aspect ratio

Introduction

The turbulent flow generally occurs in natural rivers, diversion channels and artificial canals, with quasi-sequential structures, as an inherent feature of the turbulent flow. According to the Theodorsen's wall turbulent horseshoe vortex model, these structures[1] include three parts, i.e., the streamwise vortex, the spanwise vortex, and high and low velocity strips. Adrian et al.[2-3] developed a hairpin vortex model. The hairpin vortex is generated by the disturbance near the undersurface of the channel, which has a certain replication ability with a similar longitudinal motion speed and a similar vertical motion speed, to form vortex clusters upstream and downstream, to be developed and evolved in different stages. In Fig. 1, the spanwise vortex is the head of the hairpin vortex[4], the streamwise vortex is the leg of the hairpin vortex; and the high and low speed bands are the interior of the hairpin vortex. Studying the spanwise vortices enables us to better understand the turbulence in the open channel flows.

The development of the velocity measurement techniques in recent years, such as the particle image velocimetry (PIV), makes it feasible to study the spanwise vortices based on the flow field data[5-6]. The second generation vortex identification technique has some shortcomings (e.g., the threshold selection is without a universal rule, strong and weak vortices cannot be identified at the same time)[7]. The UTA team (University of Texas at Arlington) discovered a physical measure to quantitatively describe the rigid rotating part of the fluid–the Liutex vector[8]. Based on that, the third generation Omega-Liutex vortex identification method is developed[9]. Compared with the second-generation vortex identification method, the third generation has the merits of clear physical meaning, insensitive to threshold selection, and the ability to simultaneously identify strong and weak vortices[7]. In this study, a high-frequency and high-resolution PIV is used to measure the flow parameters of the uniform flow turbulence in the open channel under seven different conditions. The third generation

---

Project supported by the Major Program of the National Natural Science Foundation of China (Grant No. 51527809), the Research Project of China Three Gorges Corporation (Grant No. 0704106).
Biography: Bin Li (1995-), Male, Master,
E-mail: libin2014520@outlook.com
Corresponding author: Wen-jun Yang,
E-mail: yangwj@mail.crsri.cn

vortex identification method of the Omega-Liutex is applied to accurately identify the spanwise vortices.

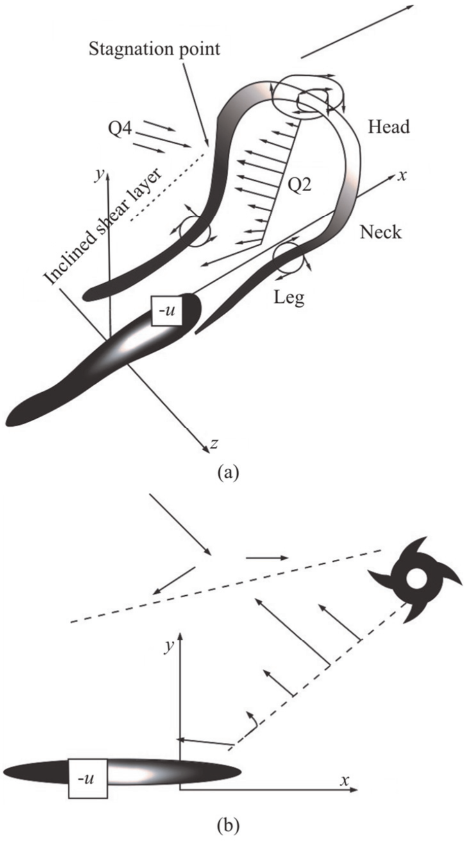

Fig. 1 Schematic diagram of hairpin vortex model[3]

1. Experimental details

1.1 *Test program*

A transparent plexiglass water tank (with a length of 14.00 m, a width of 0.30 m and a height of 0.25 m) is used. The bed slope is adjustable. In this paper, u and v are the horizontal and vertical components of the flow velocity, respectively. A total of seven sets of constant uniform flow experiments (with Reynolds number in the range of 5 241-25 507) are conducted. The Froude number of the flows (slow and rapid flows) is in the range of 0.64-1.47. Detailed parameters of the experiments are presented in Table 1. S is the bed slope of the flume, B is the width of the flume, H is the water depth and U_m is the time averaged flow velocity. The Reynolds number is expressed as $Re = HU_m / \nu$, where ν is the kinematic viscosity coefficient. The friction Reynolds number is expressed as $Re_* = Hu_* / \nu$, where u_* is the friction velocity. For all test groups, the water temperature is maintained at 17.9°C.

1.2 *Setting parameters of PIV*

In the measurements, a set of high-frequency and high-resolution PIV developed by Tsinghua University is used. The rated power of the dual-pulse laser is 20 W and the thickness of the sheet light source is about 1 mm. The PSP tracer particles with a diameter of 5 μm are distributed in the flow. The images of the flow field in the streamwise direction are taken. JFM2019 version software developed by Tsinghua University is applied to calculate the two-dimensional flow field. During the flow field sampling, the camera works in the trigger mode to perform independent sampling in order to ensure the independence of two adjacent instantaneous flow images. Frequency is denoted by f (the number of flow fields obtained per second). A pair of images are taken every second to calculate the flow field. The time interval between a pair of images is Δt, and the particle displacement within Δt is less than a quarter of the interpretation window, which is adjusted according to the flow rate. Detailed shooting parameters of PIV are presented in Table 2. Each group of data contains 4 900 (N_f) pairs of images to obtain 4 900 independent flow fields. The exposure time δt of each image is set to 100 μs, which ensures the brightness and avoids tailing. A 16×16 pixel interpretation window is used for the PIV data post-processing, and the overlap rate is 50% to obtain a grid with a vertical spacing of 8 pixels.

2. The Omega-Liutex identification method

2.1 *Basic algorithms of identification method*

The third generation Omega-Liutex identification method combines the Liutex method[10-11], the Omega

Table 1 Hydraulic parameters of experiments

Group	S	H /10^{-2}m	$B \cdot H^{-1}$	U_m /(10^{-2}m·s^{-1})	Fr	Re	Re_*
T1	0.0006	1.97	15.20	28.15	0.64	5 241	200
T2	0.0010	2.40	12.50	30.86	0.64	6 988	347
T3	0.0010	3.04	9.87	36.86	0.67	10 482	495
T4	0.0020	3.25	9.22	46.68	0.83	1 4326	775
T5	0.0006	4.05	7.40	47.51	0.75	18 169	590
T6	0.0035	2.13	14.06	46.01	1.01	9 259	544
T7	0.0050	3.25	9.22	83.11	1.47	25 507	1 225

Table 2 Shooting parameters of PIV

Group	R_s /pixel·mm^{-1}	Size (Length×width)	δt /μs	f /Hz	Δt /μs	N_f
T1	15	1 008×296	100	1	2 660	4 900
T2	15	1 136×360	100	1	2 119	4 900
T3	15	1 024×456	100	1	1 799	4 900
T4	15	976×488	100	1	1 500	4 900
T5	15	1 360×608	100	1	1 500	4 900
T6	15	1 104×320	100	1	1 500	4 900
T7	15	1 200×488	100	1	850	4 900

method[12-13]. A derivation of this method is as follows

$$\nabla V_{\theta \min} = \begin{bmatrix} \lambda_{cr} & -(\beta-\alpha) & 0 \\ \beta+\alpha & \lambda_{cr} & 0 \\ \xi & \eta & \lambda_r \end{bmatrix} + \begin{bmatrix} \lambda_{cr} & \alpha & \frac{1}{2}\xi \\ \alpha & \lambda_{cr} & \frac{1}{2}\eta \\ \frac{1}{2}\xi & \frac{1}{2}\eta & \lambda_r \end{bmatrix} + \begin{bmatrix} 0 & -\beta & -\frac{1}{2}\xi \\ \beta & 0 & -\frac{1}{2}\eta \\ \frac{1}{2}\xi & \frac{1}{2}\eta & 0 \end{bmatrix} = A + B \tag{1}$$

The original definition of Ω is

$$\tilde{\Omega}_{3D} = \frac{\beta^2 + \frac{1}{4}(\xi^2+\eta^2)}{\beta^2 + \frac{1}{2}(\xi^2+\eta^2) + \alpha^2 + \lambda_{cr}^2 + \frac{1}{2}\lambda_r^2 + \varepsilon} \tag{2}$$

where $(\xi^2+\eta^2)$ denotes the shear effect, not so much the effect of the fluid rotation. The effect of the shear is removed from the Omega-Liutex vortex identification method, namely

$$\tilde{\Omega}_R = \frac{\beta^2}{\beta^2 + \alpha^2 + \lambda_{cr}^2 + \frac{1}{2}\lambda_r^2 + \varepsilon} \tag{3}$$

where $\beta = 1/2\boldsymbol{\omega}\cdot\boldsymbol{r}$, $\alpha = 1/2\sqrt{(\boldsymbol{\omega}\cdot\boldsymbol{r})^2 - 4\lambda_{ci}^2}$.

Liutex is based on the rigid rotation part of the local fluid motion in the flow field in the same direction as the real eigenvector of the velocity gradient tensor. It represents the local axis, and the magnitude is the rigid rotation angular velocity. The explicit equation is

$$\boldsymbol{R} = R\boldsymbol{r} \tag{4}$$

where $R = \boldsymbol{\omega}\cdot\boldsymbol{r} - \sqrt{\boldsymbol{\omega}\cdot\boldsymbol{r}^2 - 4^2\lambda_{ci}}$.

$\tilde{\Omega}_R$ can also be expressed as

$$\tilde{\Omega}_R = \frac{(\boldsymbol{\omega}\cdot\boldsymbol{r})^2}{2[(\boldsymbol{\omega}\cdot\boldsymbol{r})^2 - 2\lambda_{ci}^2 + 2\lambda_{cr}^2 + \lambda_r^2] + \varepsilon} \tag{5}$$

where $\varepsilon = b_0(\beta^2-\alpha^2)_{\max}$, b_0 is a small positive value, and $\tilde{\Omega}_R = 0.52$.

$\tilde{\Omega}_R$ is not sensitive to the threshold, with a good ability to identify weak vortices, and to effectively measure the relative strength. Therefore, $\tilde{\Omega}_R$ is better than the Q method[7]. To ensure the accuracy of the vortex identification, the threshold $\Omega = 0.52\text{-}0.65$, can be adjusted by repeated experiments. In this paper, Ω is set to 0.58.

2.2 *Operation method and comparison*

The data processing method can be briefly described as follows: (1) The flow field obtained by the PIV is calculated and analyzed in Tecplot 360 (EX 2017 R3). (2) Ω value is calculated by the Omega-Liutex UTA program (Omega-Liutex UTA is a set of FORTRAN codes for vortex identification and related vortex and turbulence research). (3) The information about vortices can be viewed in Tecplot 360 (EX 2017 R3), and the number of the spanwise vortices in each section can be calculated by using related programs.

Figures 2, 3 and 4 are the cloud images of the structured vorticity, the rotation intensity and the Omega-Liutex, respectively. The x-axes and y-axes are the internal scales (pixel size) of the processed flow field after the PIV shooting. The position marked in dark blue in Fig. 2 indicates the existence of a vortex, while the yellow area in Fig. 3 represents a vortex. The red area in Fig. 4 denotes a vortex, and the color indicates the strength of the vortex.

Through comparison, it is found that the third generation Omega-Liutex identification method can effectively and clearly identify the vortex. Compared to the first and second-generation vortex identification technologies (e.g., the structured vortex and the rotation intensity method), the identification accuracy is effectively improved.

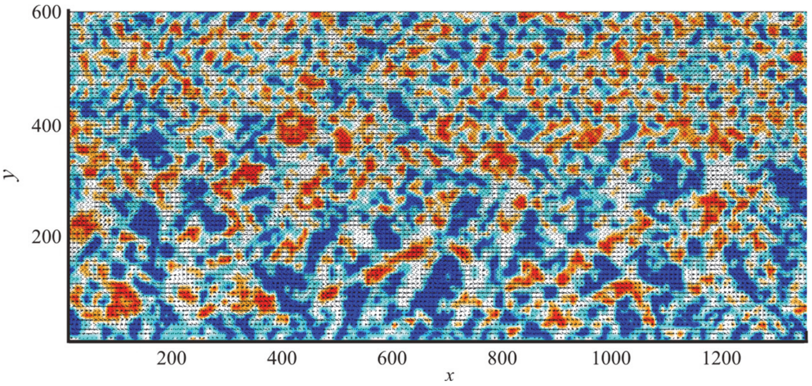

Fig. 2 (Color online) Structured vorticity cloud diagram

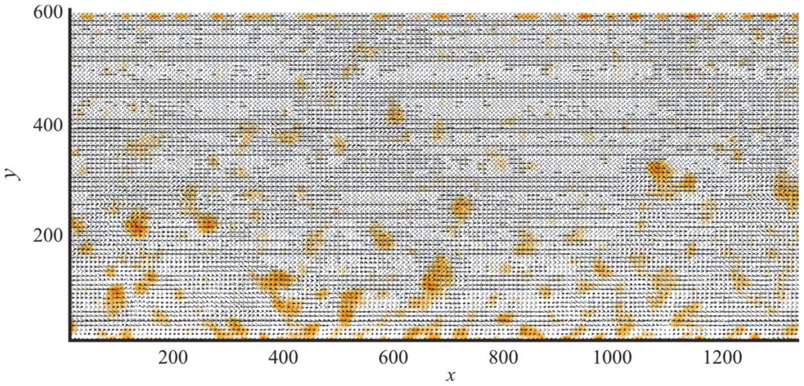

Fig. 3 (Color online) Rotating intensity cloud diagram

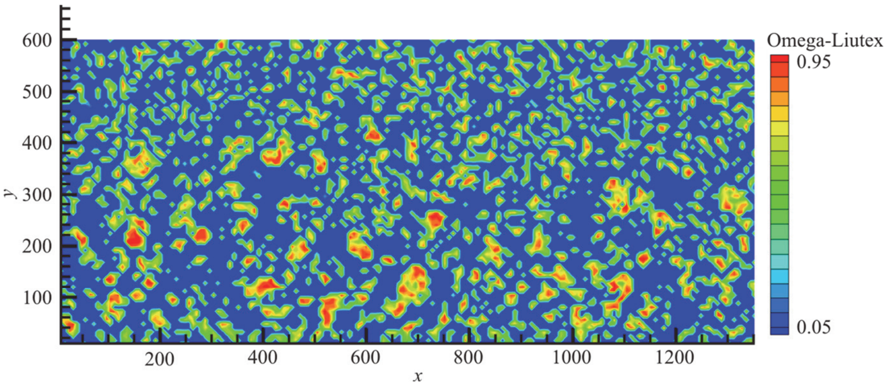

Fig. 4 (Color online) Omega-Liutex cloud diagram

3. Results and discussions

3.1 *Hydraulic characteristics*

In the flow, there is a close relationship between the velocity gradient, the turbulent intensity, the Reynolds stress and the vortex. In fact, the motion of the fluids can be decomposed into the deformation (shear) and the rotation, if ignoring the translation. When the Reynolds number is large, and the velocity gradient, the turbulence intensity, the Reynolds stress are also large, the shear layer is unstable but the rotation is linearly stable[14]. Then the fluids away from the wall, cannot very well bear the shear force, the laminar flow which is dominated by the shear and is unstable would be transferred to the turbulent flow which is dominated by the rotation and is stable, so there will be more vortices. In addition, the moment $\overline{u'v'}$ in the Reynolds stress is related to the second order of magnitude at the point and contains the information about the vortex motion.

Figure 5 shows the longitudinal time-averaged velocity distribution of seven test groups. It is shown that the horizontal velocity distribution for the flows can be described by a parabolic function in the outer region. This is consistent with the horizontal velocity distribution suggested in other studies[15-17]. Figure 6 shows the time-averaged vertical velocity distribution of seven test groups. The turbulence intensities in the streamwise and vertical directions are displayed in Figs. 7, 8, respectively. Figure 9 presents the Reynolds stress along the flow depth. From Fig. 5, it is clearly seen that the velocity is in the logarithmic distribution (except for the bed area). The streamwise turbulence intensity (Fig. 7), the vertical turbulence intensity (Fig. 8), and the Reynolds stress (Fig. 9) of the seven test groups are well correlated. At the same time, they correspond to the Reynolds number of each test group, which can accurately reflect the turbulence of the open channel[18]. These flow characteristics indicate that the experimental data are reliable.

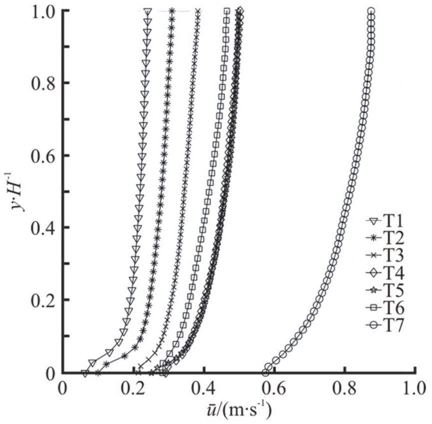

Fig. 5 Time-averaged horizontal velocity distribution of each group

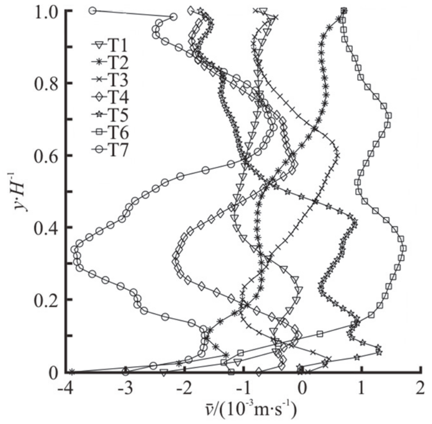

Fig. 6 Time-averaged vertical velocity distribution of each group

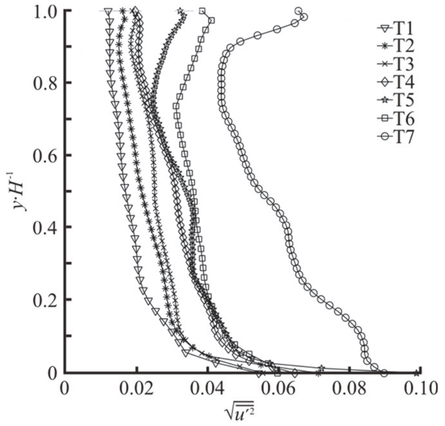

Fig. 7 Distribution of longitudinal turbulence intensity along water depth for each group

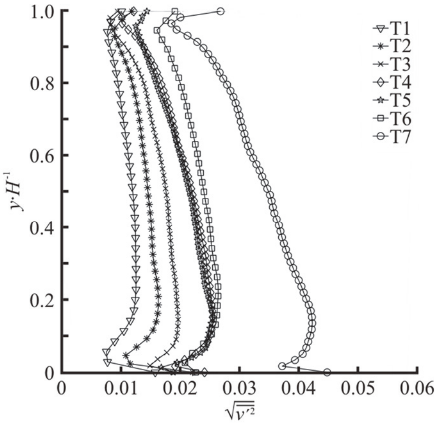

Fig. 8 Distribution of vertical turbulence intensity along water depth for each group

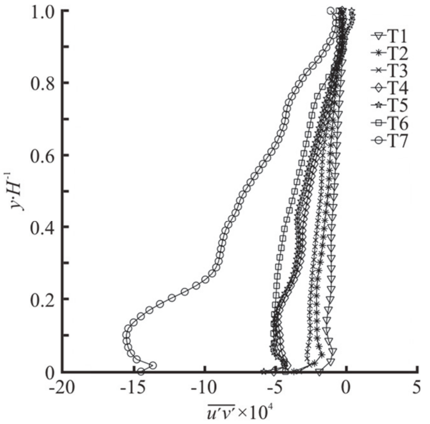

Fig. 9 Reynolds stress distribution of each group

3.2 *Analysis of the spanwise vortex density*

The spanwise vortices grow and diminish with the flow development, and there are significant differences in the number of vortices in different regions. In this study, the density of the spanwise vortices is statistically analyzed on an external scale, and the spanwise vortex density is denoted as "P" in this study. The unit of the spanwise vortex density is "n /m²", "n" represents the number of the spanwise vortices. Figure 10 displays the spanwise vortex density distributions of different test groups. In this figure, there are significant differences in the spanwise vortex density of different groups. Among them, three groups (i.e., T4, T5 and T6) contain different aspect ratios, while the water flow velocity remains similar. Under the working conditions of the three groups, the horizontal time average velocity difference is small. Nevertheless, the difference can be huge in the spanwise vortex density because it increases with the increase of the aspect ratio. The spanwise vortex density is the highest at the shallow water depth and the high Reynolds number (T6). On the contrary, the spanwise vortex density is the lowest at the deep water depth and the low Reynolds number (T5). It can be concluded that, with different aspect ratios, the approximate averaged flow velocity of the testing section can influence the spanwise vortex density. Notably, the streamwise turbulence intensity (Fig. 7), the vertical turbulence intensity (Fig. 8) and the Reynolds stress (Fig. 9) of these three test groups do not have much difference. This indicates a significant difference in the vortex density distribution along the water depth.

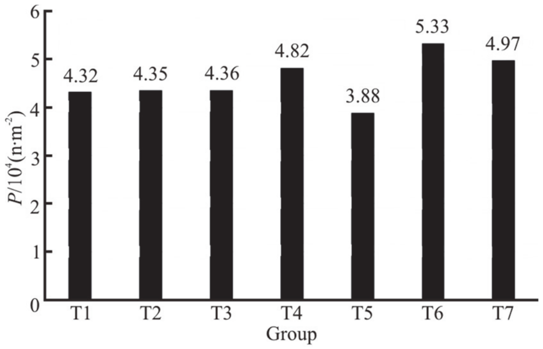

Fig. 10 Distribution of vortex density of each group

Figure 11 displays the distribution trend of the spanwise vortex density of each group along the flow depth. Each group is divided into 10 layers along the vertical direction, and the middle position of each layer is regarded as the measuring point. The trend of each testing group is basically the same. The spanwise vortex density reaches the highest level at the position where $y/H = 0.1 - 0.2$, and then declines. This finding is basically consistent with the experimental data of Wu and Christensen[19] in channel and boundary layer flows. By comparing Figures 8, 9 and 11, it is seen that the distribution pattern of the spanwise vortex density curves along the vertical direction of each group is quite similar to those of the vertical turbulence intensity and the Reynolds stress. The absolute values of the Reynolds stress and the vertical turbulence intensity reach the peaks at the position $y/H = 0.1$. The vortex density also reaches its highest level at $y/H = 0.1 - 0.2$, and then declines. This is consistent with what would be predicted by the turbulence dynamics. In addition, Fig. 7 shows that the longitudinal turbulence intensity exhibits a downward trend with the increases of y/H value, which is similar to the general trend that the spanwise vortex density decreases with the decrease of the flow depth. In Fig. 11, the test groups T3, T4 and T7 have a similar aspect ratio, but different Reynolds numbers. The group with higher velocity at the same depth has a higher vortex density than other groups. The main reason is that as the horizontal velocity increases, the horizontal velocity gradient is magnified, the shear action strengthens, the shear layer is more unstable, the water turbulence intensity and the Reynolds stress become larger, and the turbulence conditions are good, so the number of the spanwise vortices is larger.

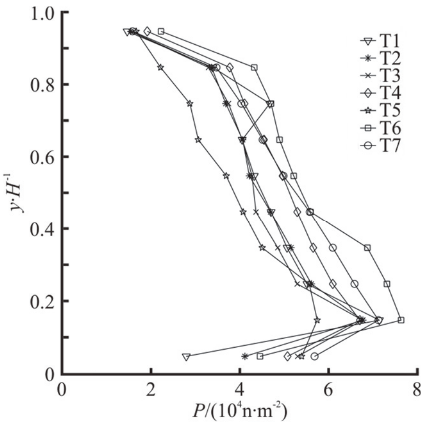

Fig. 11 Vortex density of each group is distributed along the vertical line

It is noted that the vortex density reaches its peak at $y/H = 0.1 - 0.2$, corresponding to the maximum Reynolds stress of each group around $y/H = 0.1$. The hairpin vortex originates from small disturbances with jet characteristics near the bed area. In the area where the transition zone and the logarithmic zone meet, the Reynolds stress is high because of the strong shearing effect, and the jetting occurs frequently. Therefore, the hairpin vortex group can achieve its full growth and development. When $y/H > 0.2$, the vortex density begins to drop slowly with the increase of y/H value. In this regard, as the horizontal velocity gradient and the Reynolds stress become smaller, the shear layer becomes more stable, the number of vortices decreases, and the strength of the vortex decreases, causing the vortices to disappear faster. On the other hand, as y/H increases, the vortex scale increases, and the distance between the vortices becomes smaller, which leads to the merging of the vortices and reduces the number of the vortices[20].

In Fig. 11, at $y/H = 0.9\text{-}1.0$, the vortex density of each group drops rapidly. On one hand, at $y/H = 0.9$, the horizontal velocity gradient decreases, the vertical turbulence intensity decreases rapidly, and the Reynolds stress decreases. These are not conducive to the formation of the spanwise vortices. On the other hand, the disturbance of the flow surface causes the turbulence intensity to magnify near the free surface, and the vortex is easily broken into small vortices near the surface[21] These lead to the rapid disappearance of the spanwise vortices. Studies also show that the decrease of the number of the spanwise vortices near the surface is slower than on the outer boundary of the boundary layer flow, which may be related to the complex volatility of the water surface caused by the influence of the side wall. In addition, due to the influence of the air shearing and the secondary flow, the dynamic characteristics of the turbulence near the water surface can be complex. These can affect the formation and the survival of the spanwise vortex. The above-mentioned mechanisms can lead to the difference in the reduction speed of the spanwise vortex near the turbulent water surface of an open channel. Thus further investigations would be needed for the specific mechanism.

4. Conclusions

Using the high spatio-temporal resolution PIV, seven different flow conditions are chosen in the open water channel. The large-capacity sample collection is made on the $x\text{-}y$ section, and a total of 4 900 double snapshots for each group are obtained. Using the third generation Omega-Liutex vortex identification method, the spanwise vortices are identified from the flow field. The quantitative characteristics of the spanwise vortex combined with the turbulence statistical parameters are analyzed. The findings of this study include:

(1) The third generation Omega-Liutex vortex identification method can effectively and accurately identify the spanwise vortices, the strong and weak vortices at the same time.

(2) For different aspect ratios, section velocities, Reynolds numbers, bed slopes, and Froude numbers, the distribution of the spanwise vortex density in the vertical direction shows similar trend. This trend is positively correlated with the turbulence intensity and the Reynolds stress.

(3) For a given aspect ratio, the number of the spanwise vortices increases with the increase of the flow velocity. The spanwise vortex density is different in different water depth, reaching the maximum at $y/H = 0.1\text{-}0.2$, and then declining.

This paper presents a research of the distribution of the spanwise vortices in open channel turbulent flows. However, there are still some unsolved challenges: (1) The detailed analysis of the size and the circulation characteristics of the spanwise vortices remains to be made, (2) The influence of the air-liquid interface and the side wall in the surface area on the distribution of the velocity needs a further study.

Acknowledgement

This work was accomplished by using the code Omega-Liutex UTA which was released by Chaoqun Liu at the University of Texas at Arlington.

References

[1] Robinson S. K. Coherent motions in the turbulent boundary layer [J]. *Annual Review of Fluid Mechanics,* 1991, 23: 601-639.

[2] Adrian R. J. Hairpin vortex organization in wall turbulence [J]. *Physics of Fluids*, 2007, 19(4): 413016.

[3] Adrian R. J., Meinhart C. D., Tomkins C. D. Vortex organization in the outer region of the turbulent boundary layer [J]. *Journal of Fluid Mechanice*, 2000, 422: 1-54.

[4] Charkrit S., Shrestha P., Liu C. Liutex core line and POD analysis on hairpin vortex formation in natural flow transition [J]. *Journal of Hydrodynamics*, 2020, 32(6): 1109-1121.

[5] Steffler P. M., Rajaratnam N., Peterson A. W. LDA measurements in open channel [J]. *Journal of Hydraulic Engineering, ASCE*, 1985, 111(1): 119-130.

[6] Vétel J., Garon A., Pelletier D. Vortex identification methods based on temporal signal-processing of time-resolved PIV data [J]. *Experiments in Fluids*, 2010, 48(3): 441-459.

[7] Liu C. Liutex-third generation of vortex definition and identification methods [J]. *Acta Acrodynamica Sinica*, 2020, 38(3): 413-431, 478.

[8] Gao Y., Liu C. Rortex and comparison with eigenvalue-based vortex identification criteria [J]. *Physics of Fluids*, 2018, 30(8): 085107.

[9] Liu C., Xu H., Cai X. et al. Liutex and its applications in turbulence research [M]. Amsterdam, The Netherlands: Elsevier, 2021, 119-149.

[10] Liu C., Gao Y., Tian S. et al. Rortex-A new vortex vector definition and vorticity tensor and vector decompositions [J]. *Physics of Fluids*, 2018, 30(3): 035103.

[11] Gao Y. S., Liu J. M., Yu Y. et al. A Liutex based definition and identification of vortex core center lines [J]. *Journal of Hydrodynamics*, 2019, 31(3): 445-454.

[12] Liu C., Wang Y. Q., Yang Y. et al. New omega vortex identification method [J].*Science China Physics, Mechanics and Astronomy*, 2016, 59(8): 684711.

[13] Wang Y., Liu C., Gao Y. Letter: Galilean invariance of Rortex [J]. *Physics of Fluids*, 2018, 30(11): 111701.

[14] Liu C., Yan Y., Lu P. Physics of turbulence generation and sustenance in a boundary layer [J]. *Computers and Fluids*, 2014, 102: 353-384.

[15] Sarma K. V. N., Prasad B. V. R., Sarma A. K. Detailed study of binary law for open channels [J]. *Journal of Hydraulic Engineering, ASCE*, 2000, 126(3): 210-214.

[16] Huai W., Hu Y., Zeng Y. et al. Velocity distribution for open channel flows with suspended vegetation [J]. *Advances in Water Resources*, 2012, 49: 56-61.

[17] Huai W., Wang W., Hu Y. et al. Analytical model of the mean velocity distribution in an open channel with double-layered rigid vegetation [J]. *Advances in Water Resources*, 2014, 69: 106-113.

[18] Wang W. E., Liao W., Qi L. J. Experiment of turbulent characteristics of flow in wide-and-narrow channels [J]. *Advances in Water Science*, 2020, 31(3): 394-403(in Chinese).

[19] Wu Y., Christensen K. T. Population trends of spanwise vortices in wall turbulence [J]. *Journal of Fluid Mechanics*, 2006, 568: 55-76.

[20] Tomkins C. D., Adrian R. J. Spanwise structure and scale growth in turbulent boundary layers [J]. *Journal of Fluid Mechanics*, 2003, 490: 37-74.

[21] Nagaosa R. Direct numerical simulation of vortex structures and turbulent scalar transfer across a free surface in a fully developed turbulence [J]. *Physics of Fluids*, 1999, 11(6): 1581-1595.